

# Knowledge-Based Anisotropic Diffusion of Vector-Valued 4-Dimensional Cardiac MR Images

Gerardo I. Sánchez-Ortiz, Daniel Rueckert and Peter Burger  
Department of Computing, Imperial College, London SW7 2BZ.\*

**Abstract.** We present a general formulation for a new knowledge-based approach to anisotropic diffusion of multi-feature and multi-dimensional images, with an illustrative application to cardiac MRI. We incorporate all available information through a more complete definition of the conductance function which differs from previous approaches in two aspects. First, we model the conductance as an explicit function of the position and not only of the differential geometry of the image data. Inherent properties of the system (such as geometrical features or non-homogeneous data sampling) can therefore be taken into account by allowing the conductance values to depend on the location in the spatial and temporal coordinate space. Secondly, by defining the conductance as a second rank tensor, the non-homogeneous diffusion equation gains a truly anisotropic character which is essential to emulate and handle certain aspects of complex data systems. We demonstrate the efficiency of the proposed framework using density and velocity encoded cine volumetric MR images of the left ventricle. In this example we incorporate into the diffusion process spatial and temporal knowledge about the shape and dynamics of the heart. The method presented is suitable for image enhancement and also for segmentation. We compare our results to those obtained with other anisotropic diffusion methods.

## 1 Introduction

Image processing and computer vision have traditionally dealt with problems like image segmentation (*i.e.* dividing an image into a certain number of meaningful regions) in cases where the data can be expressed as a single- or vector-valued *image function* defined on a  $n$ -dimensional image domain. However, in almost any image acquisition method the original signal which is to be measured is affected by noise, blurring, discretisation errors, non-linear sensor responses or any other type of misregistration that degrades the data quality.

Many semantic interpretations, like edges in an image, rely on the extraction of geometric features, e.g. differential invariants (chapter 1 in [1]). The problem of determining at which scales these image features should be measured has emerged as one of the central problems. In recent years many different approaches for image descriptions based on geometry-driven diffusion processes have been developed [1]. The concept of geometry-driven diffusion has its roots in the idea of analysing images at varying levels of resolution and was originally developed by Koenderink [2] and Witkin [3]. Koenderink has pointed out that this blurring can be expressed in terms of the heat conduction or diffusion equation:

$$\frac{\partial I(x, y)}{\partial \tau} = \nabla \cdot c \nabla I(x, y), \quad (1)$$

where  $\nabla$  is the gradient operator and  $\nabla \cdot$  is the divergence one. If the conductance term  $c$  is a constant then the diffusion process is called *isotropic*. In this case the Gaussian function  $G$  is the solution to the diffusion equation and any diffused image can be obtained directly

---

\*E-Mail: giso@doc.ic.ac.uk      URL: <http://www-asds.doc.ic.ac.uk/~giso>

by a spatial convolution with the Gaussian function, *i.e.*,  $L(x, y, \sigma) = I(x, y) \otimes G(x, y, \sigma)$ . This leads to some disadvantages: First, the filtering is linked with loss of information about image features such as objects and their boundaries. Secondly, the blurring leads to a degradation of the localization of the surviving image features.

To avoid these problems, Perona and Malik [4] have proposed a space-variant blurring which leads to the anisotropic diffusion equation

$$\frac{\partial I(x, y)}{\partial \tau} = \nabla \cdot ( c(x, y) \nabla I(x, y) ), \quad (2)$$

where the conductance is a monotonically decreasing function of the magnitude of the gradient of the intensity:

$$c = g(\|\nabla I\|) = \frac{1}{1 + (\frac{\|\nabla I\|}{k})^2}. \quad (3)$$

A conductance function defined in this manner weakens the diffusion process for values of the gradient of the intensity larger than a parameter  $k$ . As a consequence the conductance function allows diffusion at edges with low gradient values (which are presumed to be spurious edges) and prevents diffusion at edges with high gradient values (which are presumed to be significant edges). This method has been proved useful and work has been done to extend it in many areas including to vector-valued images (chapter 4 in [1]).

However, we notice that previous approaches rely only on the differential structure of the data while ignoring the particular properties of the system. As a consequence results are still poor in regions of the images with low contrast and low signal-to-noise ratio, where the differential characteristics of data do not provide the required information. Moreover, most works oversimplify the conductance function of the diffusion process, ignore the direction of the gradient, and oversee important system characteristics such as non-homogeneous data sampling.

In this article we propose a second rank tensor conductance function with an explicit dependence on the space coordinates and the data function. This tensor modifies the nature of the equations making them heterogeneous and anisotropic from the starting point, not as a consequence of the discretisation scheme as is the case of previous works. Furthermore, we develop a general framework to incorporate *a priori* knowledge of the system in multi-feature and multi-dimensional images. We illustrate this approach with an application to cine volumetric and velocity encoded magnetic resonance images of the heart, where noise reduction in data and pre-segmentation of the myocardium is commonly required.

## 2 4D Multi-Feature MRI Data

Electrocardiographically synchronized cine Magnetic Resonance Imaging (MRI) techniques can be used to generate a sequence of tissue density ( $\rho$ ) tomographic images of the heart. The sequence of images correspond to different times distributed during a cardiac cycle, covering most phases of a heartbeat. In addition to these sequences of 2-dimensional images (with which we align the  $x$ - $y$  plane of the cartesian coordinates reference system), multi-slice imaging can provide contiguous images parallel to the  $x$ - $y$  plane, at different heights in a third spatial coordinate-axis ( $z$ ). A common procedure for evaluating left ventricle (LV) performance is to produce data such that  $x$  and  $y$  lie on the short-axis plane of the LV, and  $z$  goes on the direction of the LV long-axis (as will be seen below in figure 1).

For each of the density images, velocity encoded data of the same anatomic plane of the ventricle is produced using a phase-sensitive MRI technique. The velocity data is rendered

as 3 images,  $V_x$ ,  $V_y$  and  $V_z$ , that correspond to the cartesian components of the velocity vector field  $\mathbf{V}$ .

We describe the data used as the vector function  $\mathbf{F} = \mathbf{F}(\mathbf{p}) = (F_1(\mathbf{p}), \dots, F_n(\mathbf{p}), \dots, F_N(\mathbf{p}))$  where  $\mathbf{F} : \mathfrak{R}^M \rightarrow \mathfrak{R}^N$ ,  $F_n : \mathfrak{R}^M \rightarrow \mathfrak{R}$ ,  $\mathbf{p} = (p_1, \dots, p_m, \dots, p_M)$ , and  $p_m \in \mathfrak{R}$  (*i.e.*  $\mathbf{p} \in \mathfrak{R}^M$ ). In our case the space-time coordinates are  $x, y, z, t$  ( $M = 4$ ), and the feature images are  $\rho, V_x, V_y, V_z$  ( $N = 4$ ). Therefore the data functions take the form:

$$\mathbf{F}(\mathbf{p}) = (F_\rho(\mathbf{p}), F_{V_x}(\mathbf{p}), F_{V_y}(\mathbf{p}), F_{V_z}(\mathbf{p})) \quad (4)$$

where  $\mathbf{p} = (x, y, z, t)$ . The method described below treats the space of coordinates as non-homogeneous and takes into consideration the different scales, physical units and sampling rates of the data in each of the coordinate axes. With this general treatment of the coordinate system, we deal with  $t$  as a fourth “spatial” coordinate and allow the cine sequence to provide with extra information for the diffusion process.

### 3 Vector-Valued Multi-Dimensional Anisotropic Diffusion

In the case of this vector function of several variables that represents our 4 dimensional multi-feature data, the equation for anisotropic diffusion is

$$\frac{\partial \mathbf{F}(\mathbf{p})}{\partial \tau} = \nabla \cdot (\mathbf{C}(\mathbf{p}, \mathbf{F}) \nabla \mathbf{F}(\mathbf{p})), \quad (5)$$

*i.e.* the set of the 4 coupled equations:

$$\left\{ \frac{\partial F_n(\mathbf{p})}{\partial \tau} = \nabla \cdot (\mathbf{C}(\mathbf{p}, \mathbf{F}) \nabla F_n(\mathbf{p})), \quad \text{for all } n \in \{\rho, V_x, V_y, V_z\}. \right. \quad (6)$$

We must distinguish between the variables  $t$  and  $\tau$ . While the former is the time during a heartbeat and one of the coordinates in our 4D set of data, the latter refers to the time during the diffusion process (in fact, in the case of isotropic diffusion, the total diffusion time  $\tau_{total}$  is proportional to  $\sigma^2$  where  $\sigma$  is the standard deviation of the Gaussian smoothing kernel [5]).

#### 3.1 Conductance Function

The coupling term for these equations is the inhomogeneous and anisotropic conductance function matrix defined by the product

$$\mathbf{C}(\mathbf{p}, \mathbf{F}) = \mathbf{G}(\mathbf{F}) \mathbf{W}(\mathbf{p}). \quad (7)$$

The conductance function that we introduce here differs from previous definitions in two aspects. First, in contrast to other approaches [4, 6, 7], this conductance function depends not only on the local behaviour of the data function  $\mathbf{F}$  which is subject to noise, but also on the particular characteristics of the system at every location  $\mathbf{p}$  of the 4-dimensional coordinate space. The two factors that regulate the conductance — and therefore the diffusion — are, on the one hand, the function matrix  $\mathbf{G}(\mathbf{F}(\mathbf{p}))$  that uses information obtained from the local behaviour of the data values, and on the other hand, the weighting function matrix  $\mathbf{W}(\mathbf{p})$  obtained from *a priori* knowledge of the geometry and dynamics of the system from which the data is generated, but independent of the data itself.

The second difference is that we define the conductance function as a second rank tensor, not as the scalar function normally used, therefore allowing real heterogeneous and anisotropic diffusion, result of the properties of the conductance function and not only of the data gradient of equation 5<sup>1</sup>.  $\mathbf{C}$ ,  $\mathbf{W}$  and  $\mathbf{G}$ , which expressed in matrix notation take the form  $C_{ij}, W_{ij}, G_{ij} : \mathbb{R}^4 \rightarrow \mathbb{R}$  where  $i, j \in \{x, y, z, t\}$ , permit the conductance to vary not only accordingly to the location in the space (heterogeneously) but also depending on the orientation (anisotropically).

Although in this work we only examine the simple case in which the matrices are diagonal (the elements will be computed below), a conductance function defined in this manner permits the diffusion process to be biased differently in every direction and in every position in space.  $\mathbf{G}$  accounts for the characteristics of the data (as we will see below  $\mathbf{G}$  could be a noise or boundary estimator), and  $\mathbf{W}$  accounts for the intrinsic properties of the space (for example, a diffusion process in which an electrical or gravitational field produces a force that: a) varies with the direction — for an anisotropic system, and b) varies with the distribution of mass or electrical charges in the material — for an heterogeneous medium).

### 3.2 Data Based Weighting: $\mathbf{G}(\mathbf{F})$

The framework used for describing the function matrix  $\mathbf{G}$  is suitable for using elaborated noise or edge estimators (for instance, a function that depends on the local direction of the gradient [8]). However, in this work we use a 4D multi-featured function analogous to the simple and widely used function  $g(\|\nabla I\|)$  on equation 3. This monotonically decreasing scalar function of the magnitude of the gradient of  $I$  (the image intensity), has the desired effect of blurring small discontinuities while sharpening edges when  $k$  is chosen adequately. The values of  $k_m$  (one for each coordinate axis) are computed using Canny's noise estimator [9]: 90% of the value of the integral of the histogram of the gradient's magnitude throughout the data. The computation is made for every iteration of the diffusion process (*i.e.*  $k_m$  varies with  $\tau$ ) and using the definition of the gradient's magnitude shown below. Thus, the elements of the diagonal matrix  $\mathbf{G}$  are defined as follows:

$$G_{mm} = g_m(\|\nabla \mathbf{F}\|_m^*) = \frac{1}{1 + \left(\frac{\|\nabla \mathbf{F}\|_m^*}{k_m}\right)^2} \quad \text{and} \quad (8)$$

$$\|\nabla \mathbf{F}\|_m^* = \left( \sum_n (s_n J_{mn})^2 \right)^{\frac{1}{2}} = \left( \sum_n \left( s_n \frac{\partial F_n}{\partial p_m} \right)^2 \right)^{\frac{1}{2}}, \quad (9)$$

for all  $m \in \{x, y, z, t\}$  and  $n \in \{\rho, V_x, V_y, V_z\}$ . Since the data function that we use is a vector valued function we must define a norm for the Jacobian matrix ( $\mathbf{J}$ ) of  $\mathbf{F}$  instead of using the magnitude of the gradient as a dissimilarity measure. In this work we use the definition shown above as an alternative to the formerly proposed Euclidean norm of  $\mathbf{J}$  [10]. Such dissimilarity measure exploits the information provided by the different data features  $F_n$  while preventing homogeneous regions in some directions to shadow steep gradients in others. The scaling constants  $s_n$  are used for standardising the units of the different data features. It is worth recalling that the matrix  $\mathbf{G}$  could be non-diagonal and therefore allow cross influence between coordinate axes. The next section describes how a weighting function for a specific problem can be chosen based on a *a priori* knowledge of the system.

<sup>1</sup>In works like that of Perona and Malik [4] the conductance is defined as an heterogeneous function over the image space, while the anisotropic character comes only as a consequence of their discretisation scheme.

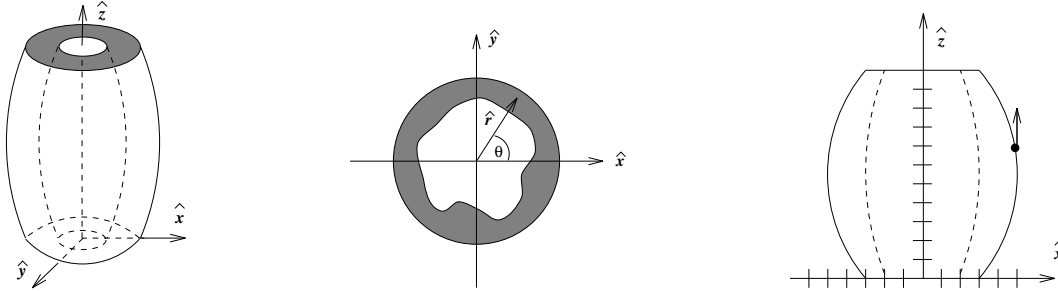


Figure 1: (a) Orientation of a barrel shaped Left Ventricle (LV) of the heart with respect to the coordinate system. (b) Cross section of the LV and polar coordinates on the  $x$ - $y$  plane. (c)  $x$ - $z$  plane view of a pixel without a myocardium neighbour in the  $z$  direction.

### 3.3 Knowledge-Based Weighting: $\mathbf{W}(\mathbf{p})$

Information about the nature of the system and the data generation process can be very valuable when processing and analysing the data. The system’s geometry and dynamics, the sources of noise in the data, and in general any kind of *a priori* knowledge can improve the results of tasks such as image segmentation or noise reduction. Using this information has a clear advantage over making statistical measurements of the regional properties of the data: the former is noise independent. However, one must find a robust method to incorporate “fresh” information from the data and thus avoid over constraining the behaviour of the system and overseeing any unexpected but real characteristics of it.

A compromise has to be made between the extent (and detail) of this information and the portability of knowledge-based methods to other systems with different characteristics. Although the use of specific knowledge about a system restricts the application of the method in other environments, a well structured formulation simplifies the incorporation of the particular characteristics of different systems to the algorithm already in use.

In the following pages we generate a weight function matrix  $\mathbf{W}(\mathbf{p})$  that reflects the characteristics of a given position within our, *per se*, anisotropic space.

#### Shape information

In the series of LV short-axis images described above, the LV muscle has a strong cylindrical symmetry (fig. 1.a). The area of interest for the segmentation, the myocardium, appears in the  $x$ - $y$  image as a ring formed by two almost concentric boundaries (fig. 1.b). The shape of the outer boundary is nearly a circle in all the slices (*i.e.* for all values of  $z$ ), and remains like that all through the heart cycle (*i.e.* for different times  $t$  in our 4D space). The shape of the inner boundary varies with time. For approximately half of the images the shape is circular and for the other half the fluctuations could be regarded as moderate deformations of a circle.

Since MRI provides high contrast between blood and tissue, the inner boundary of the myocardium can be preserved and emphasized with the part of the diffusion equation that uses the norm of the gradient of the intensity function, but the outer boundary tends to be diffused and therefore joint with regions outside the myocardium.

For these reasons we introduce the weighting factors  $W_{xx}$  and  $W_{yy}$  which acting together penalize diffusion on the  $x$ - $y$  plane, in the radial direction of an “imaginary” polar coordinate

system whose origin is located at the centre of the circle that best fits the outer boundary of the myocardium. In this manner we avoid blurring the outside boundaries of the myocardium and the regions of the inner boundary which are aligned with circles centred at the origin of such polar coordinate system (fig. 1.b).

Finding the location of the centre of such family of circles can be done immediately by inspection, or can be done automatically with a simple algorithm based on the Hough [11] transform. In any case the method described is very robust to small errors in the location of this centre, provided it is inside of both boundaries (a condition that can be easily satisfied). For this reason we use the same coordinates of the centre for all images (*i.e.* for all planes and times), overriding the small variations of 1 or 2 pixels found when computing the centre in various sample images, and therefore making the weighting functions  $W_{xx}(x, y)$  and  $W_{yy}(x, y)$  independent of the coordinates  $z, t$  (we must remember that, for example, 10 slices and 16 phases would require the process of finding the coordinates for 160 images). The analytical expressions for these weights and the ones we will describe in the text below (with some minor modifications explained at the end of this section) are shown in the next section (eqs. 14-18).

Although cylindrical coordinates  $(r, \theta, z)$  would seem a natural choice for developing the equations, the data is given in cartesian coordinates  $(x, y, z)$  and we would require interpolation to convert from one system to another. Since the interpolation could introduce unwanted blurring, we prefer to write the equations directly in cartesian coordinates.

In the third spatial direction,  $z$ , we also have *a-priori* information that can be used to improve the diffusion process. The LV wall bends along the  $z$  axis direction which is aligned with the long axis of the ventricle. In the regions of  $z$  where the bending is maximum, the correlation between pixels that form part of the myocardium in adjacent slices along  $z$  is smaller than in regions where the bending is almost non-existent, *i.e.* where the myocardium lies straight. We can imagine this in the following manner: consider the pixels corresponding to the myocardium in the out-most region of the  $x-y$  plane where the bend of the LV wall along the  $z$  axis is maximum (see fig. 1.c). Neighbouring pixels in the  $z$  direction, *i.e.* in the adjacent  $x-y$  slices, probably do not belong to the myocardium but to a different kind of tissue and therefore they should be excluded from the diffusion process. On the other hand,  $x-y$  slices where the bend of the LV wall along the  $z$  axis is minimum should have high weights correlating pixels adjacent in the  $z$  direction.

The weight function  $W_{zz}(z)$  is then determined so that it fits the expected correlation between contiguous  $x-y$  slices of the 4-dimensional data. We find that a sinusoidal function can approximately describe this correlation when fixing the frequency and phase parameters of the function according to the data (this was done using long axis LV images).

### Temporal information

As for the 4th dimension, the time axis  $t$ , we can also correlate data with different weights using information about the behaviour of the heart during the heart cycle, specifically, using the fact that the LV contracts (and expands) at very different speeds during the cycle. The immediate consequence of this is that data obtained at times when the contraction rate is maximum is not very correlated with data adjacent in the  $t$  axis (the data gathered shortly before and afterwards in the cine sequence). On the contrary, data obtained when the heart is almost static should be strongly correlated in the time axis. This phenomena can be viewed as non-homogeneous data sampling.

As a first approximation to the speed vs. time relationship we generate the weight function  $W_{tt}(t)$  using a sinusoidal function that approximately describes the desired correlation between successive data.

These are the elements of the diagonal function matrix  $\mathbf{W}(\mathbf{p})$ . Although the curvature of the LV wall along the  $z$  axis is not very high — and therefore the weights  $W_{zz}$  are fairly similar along the  $z$  axis, we employ sin and cos weight functions in the 4 coordinate axes' directions. In this manner we provide the knowledge based model with symmetry that simplifies the mathematical treatment. Furthermore, without losing the main characteristics of the weighting functions, we use square sin and cos functions that simplify the computation of constants used to preserve the total flux of brightness of the 4D image (like that of eq. 19). We use adiabatic boundary conditions in the 4 coordinate axes, *i.e.* the conductance function is set to zero in the boundaries of the 4-dimensional “image”. The equations for the weight functions described here are shown in the next section.

## 4 Discrete Scheme

Equation 5 can be discretised on a hyper-cubic lattice (similar to a square one but in 4D rather than 2D), where the data value is associated with the vertices, and conduction coefficients with the arcs. Using a 4D extension of the 4-nearest-neighbours discretisation used by Perona and Malik [4], we work on 8-non-diagonal-nearest-neighbours to obtain the following scheme:

$$\mathbf{F}^\tau(\mathbf{p})|_{\mathbf{p}=\mathbf{p}_o}^{\tau=i+1} = \mathbf{F}^\tau(\mathbf{p})|_{\mathbf{p}=\mathbf{p}_o}^{\tau=i} + \lambda \left( \sum_{d \in \{E, W, N, S, U, D, A, B\}} C^d(\mathbf{p}, \mathbf{F}) \Delta^d \mathbf{F}^\tau(\mathbf{p}) \right) \Bigg|_{\mathbf{p}=\mathbf{p}_o}^{\tau=i} \quad (10)$$

Note that these are in fact 4 coupled equations since  $\mathbf{F} \rightarrow F_n$  where  $n \in \{\rho, V_x, V_y, V_z\}$ . These computations are carried out for every point of coordinates  $\mathbf{p}_o = (x_o, y_o, z_o, t_o)$  in the whole of the data's domain. The new value of  $\mathbf{F}$  (the diffused data) is calculated at every iteration step ( $\tau = i$ ) from the previous stage of the data ( $\tau = i - 1$ ). Since the matrix  $\mathbf{C}$  is diagonal, we simplify the nomenclature by introducing the direction index  $d$ . Then, the summation takes place over all the 8 neighbours' directions, namely:  $E, W$  (east and west on the  $x$  axis),  $N, S$  (north and south on the  $y$  axis),  $U, D$  (up and down on the  $z$  axis), and  $A, B$  (after and before on the  $t$  axis). The following definitions hold for the present scheme:

$$\left( \Delta^d \mathbf{F}^\tau(\mathbf{p}) \right) \Big|_{\mathbf{p}=\mathbf{p}_o}^{\tau=i} = \mathbf{F}^\tau(\mathbf{p}) \Big|_{\mathbf{p}=\mathbf{p}_o + \mathbf{d}\mathbf{p}^d}^{\tau=i} - \mathbf{F}^\tau(\mathbf{p}) \Big|_{\mathbf{p}=\mathbf{p}_o}^{\tau=i} \quad (11)$$

where  $\mathbf{d}\mathbf{p}^d = (\delta^{Ed} - \delta^{Wd}, \delta^{Nd} - \delta^{Sd}, \delta^{Ud} - \delta^{Dd}, \delta^{Ad} - \delta^{Bd})$  and  $\delta$  is the Kronecker's delta defined as  $\delta^{ij} = \begin{cases} 1 & \text{if } i = j \\ 0 & \text{if } i \neq j \end{cases}$ . The conductance function is computed as

$$C^d(\mathbf{p}, \mathbf{F}^\tau) = W^d(\mathbf{p}) g_d (\|\nabla \mathbf{F}^\tau(\mathbf{p})\|_d^*) \quad (12)$$

where  $g_d$  is that of equation 8, and equation 9 becomes

$$\|\nabla \mathbf{F}^\tau(\mathbf{p})\|_d^* = \left( \sum_n (s_n \Delta^d F_n^\tau(\mathbf{p}))^2 \right)^{\frac{1}{2}}, \quad (13)$$

for all  $d \in \{E, W, N, S, U, D, A, B\}$  and  $n \in \{\rho, V_x, V_y, V_z\}$ .  $\Delta^d$  is defined for the single valued functions  $F_n$  in a fashion similar to that of its vector homologous of equation 11. In this notation, the weights functions can be expressed as

$$W^d(\mathbf{p}) = W_{xx}^d(x, y) + W_{yy}^d(x, y) + W_{zz}^d(z) + W_{tt}^d(t) \quad (14)$$

where

$$W_{xx}^d(x, y) = (\delta^{Ed} + \delta^{Wd}) \sin^2(\theta(x, y)) \quad (15)$$

$$W_{yy}^d(x, y) = (\delta^{Nd} + \delta^{Sd}) \cos^2(\theta(x, y)) \quad (16)$$

$$W_{zz}^d(z) = (\delta^{Ud} + \delta^{Dd}) \sin^2\left(\omega_z\left(z + \frac{1}{2}(\delta^{Ud} - \delta^{Dd})\right) + \phi_z\right) \quad (17)$$

$$W_{tt}^d(t) = (\delta^{Ad} + \delta^{Bd}) \sin^2\left(\omega_t\left(t + \frac{1}{2}(\delta^{Ad} - \delta^{Bd})\right) + \phi_t\right). \quad (18)$$

The angle  $\theta(x, y) = \arctan((y - y_{origin})/(x - x_{origin}))$  is that defined by the virtual polar coordinate system whose origin is located at  $(x_{origin}, y_{origin})$ . The constants  $\omega_z, \omega_t, \phi_z, \phi_t$  are the frequencies and phases described in relation to  $\mathbf{W}$  and used to fit the weight functions to the data sets. The constant  $\lambda$  of equation 10 used for keeping the model numerically stable is computed using the average values  $\bar{w}^d$  of the weights  $W^d$  over their entire range of values:

$$\lambda = \frac{1}{\sum_{d \in \{E, W, N, S, U, D, A, B\}} \bar{w}^d} \approx \frac{1}{8 \cdot \frac{1}{2}} = \frac{1}{4}. \quad (19)$$

## 5 Results and Discussion

As we mentioned before, there are two main reasons for using diffusion on images. If the purpose of the diffusion process is to remove noise from the data and preserve details of the data, for instance when using velocity data to extract dynamical information [12, 13], then the total diffusion time must be small. However, when the purpose of the diffusion is to pre-segment the images, a much longer time is suitable. In either case the number of iterations of the process can be set interactively by inspection of the results or estimating the noise or data correlation. For example, Canny's algorithm will gradually halt the process by decreasing the value of  $k_m$ .

Some preliminary results are shown in figure 2 where we apply different types of anisotropic diffusion on MR data of the myocardium. The same diffusion times were used to produce all images. The original density image is shown in figure 2.a. Figure 2.b shows the result of the anisotropic diffusion process using standard Perona and Malik 2-dimensional anisotropic diffusion. Knowledge-based multi-feature anisotropic diffusion results are shown for 2- and 4-dimensional data in figures 2.c and 2.d respectively. Although standard anisotropic diffusion preserves and sharpen some edges, it can make disappear some others (fig. 2.b). From the above mentioned diffusion processes, only those shown in figures 2.c and 2.d preserve the left side of the external boundary, the gap near to the bottom left corner, and the structure of the papillary muscles (the 2 protuberances of the inner boundary).

Figures 3.a-c compare the magnitude of gradient of the original with the diffused images along the horizontal line at the centre of the images. In these profiles we can see that the left external boundary, which appears as the leftmost protuberance, is preserved only in the proposed diffusion schemes. We must notice that this is not a consequence of shorter *effective* diffusion times of the weighted schemes in relation to standard anisotropic diffusion. The coefficients  $\lambda$  for each diffusion scheme compensate for the schemes' different number of pixel neighbours and knowledge based weights which influence the total flux of brightness. Our experiments have verified this and showed that for standard anisotropic diffusion, shorter diffusion times in which important boundaries are preserved, are not long enough to smooth homogeneous regions and sharpen prominent edges.

In figure 3.c we can also appreciate how the second peak from the right has been detected but shifted from the original image. This highlights the use of multi-feature and

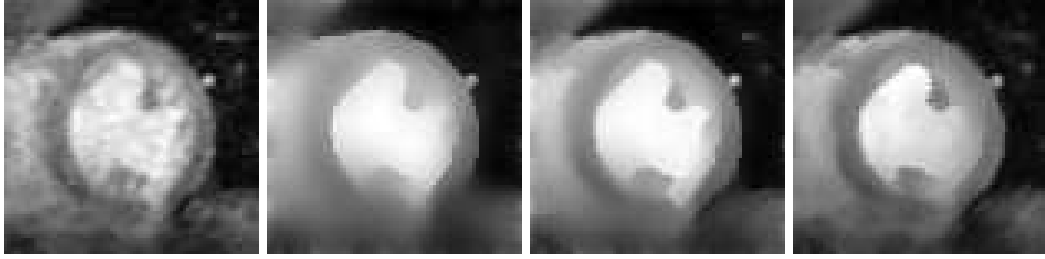


Figure 2: Preliminary results on a density MR image of the myocardium: (a) original image, (b) standard 2D Anisotropic Diffusion (AD), (c) knowledge-based multi-feature 2D AD, (d) knowledge-based multi-feature 4D AD.

4-dimensional information that helps to locate a feature landmark using information that can not be seen in the image (since it belongs to other contiguous images). We must remember that we are working with a 4-dimensional “body” and we can only visualize 2D images.

Two fundamental aspects of this model are introduced by making  $\mathbf{C}$  a matrix and an explicit function of the position, and not only of the gradient. First, an explicit function of the position can treat the space as heterogeneous and therefore incorporate the any available knowledge about the system (forcing the diffusion to be zero at the boundaries, as most models do, is already an example of an inhomogeneous space). Secondly, making  $\mathbf{C}$  a matrix we allow the model to bias different directions in the coordinates’ space, making the conductance truly anisotropic and permitting the use of known symmetries to improve the results of the diffusion.

We are currently comparing our method with other geometry driven diffusion schemes [8] [14]. However, at present it appears that these methods are not well suited for multi-valued images like those described here. Although in this work we make little use of the dynamical information provided by the velocity data, at present we are trying to incorporate this knowledge into the diffusion process. Our results will be extended in a forthcoming paper.

## References

- [1] B.M. ter Haar Romeny (Ed.). *Geometry-Driven Diffusion in Computer Vision*. Computational Imaging and Vision. Kluwer Academic Publishers, 1994.
- [2] J. J. Koenderink. The structure of images. *Biological Cybernetics*, 50:363–370, 1984.
- [3] A. Witkin. Scale-space filtering. In *Int. Joint Conf. on Artif. Intell.*, pages 1019–1022, 1983.
- [4] P. Perona and J. Malik. Scale-space and edge detection using anisotropic diffusion. *IEEE Transactions on Pattern Analysis and Machine Intelligence*, 12(7):629–639, July 1990.
- [5] L. Alvarez, P. L. Lions, and J. M. Morel. Image selective smoothing and edge detection by nonlinear diffusion II. *SIAM Journal of Numerical Analysis*, 29(3):845–866, June 1992.
- [6] R. T. Whitaker. Geometry-limited diffusion in the characterization of geometric patches in images. *CVGIP: Image Understanding*, 57(1):111–120, January 1993.
- [7] G. Gerig, O. Kübler, R. Kikinis, and F. A. Jolesz. Nonlinear anisotropic filtering of MRI data. *IEEE Transactions on Medical Imaging*, 11(2), 221-231 1992.

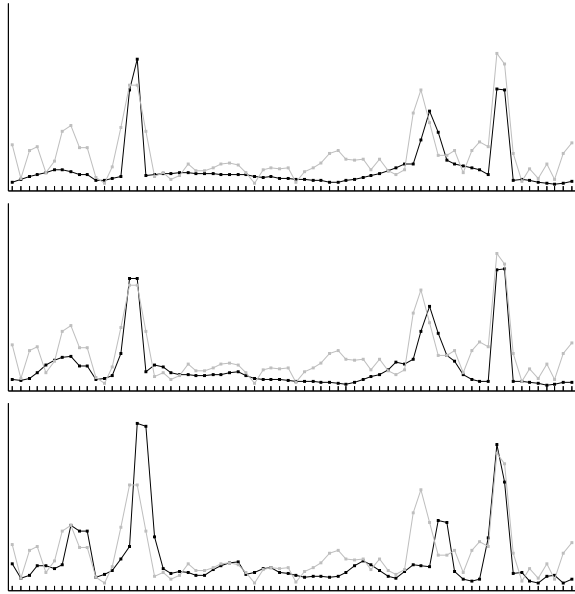


Figure 3: Black curves are the profiles of the magnitude of the gradients on a horizontal line at the centre of the diffused images of figure 2: (a) standard 2D AD (fig. 2.b), (b) knowledge-based multi-feature 2D AD (fig. 2.c), (c) knowledge-based multi-feature 4D AD (fig. 2.d). The grey curve in all plots correspond to the profile of the magnitude of the gradient of the original image (fig. 2.a). Notice that the proposed diffusion schemes (shown in (b) and (c)) have successfully preserved the left external boundary that appears as the leftmost protuberance of the black curves. Notice also that the shift of some peaks in (c) is not an error: the 4D method locates the boundaries by using information belonging to contiguous images that are not shown in the figures.

- [8] G.Z. Yang, P. Burger, D.N. Firmin, and S.R. Underwood. Structure Adaptive Anisotropic Filtering for Magnetic Resonance Image Enhancement. In *Computer Analysis of Images and Patterns (CAIP)*, Prague, 1995.
- [9] J. Canny. A computational approach to edge detection. *IEEE Transactions on Pattern Analysis and Machine Intelligence*, 8(6):679–698, 1987.
- [10] R. Whitaker and G. Gerig. Vector-valued diffusion. In B.M. ter Haar Romeny (Ed.) [1], chapter 4, pages 93–134.
- [11] D.H. Ballard. Generalizing the Hough transform to detect arbitrary shapes. *Pattern Recognition*, 13(2):111–122, 1981.
- [12] G.I. Sanchez-Ortiz and P. Burger. Vector Field Analysis of the Dynamics of the Heart using Velocity Encoded NMR Images. In *9th International Symposium on Computer Assisted Radiology, CAR'95*, pages 228–233, Berlin, June 21-24 1995. Springer Verlag.
- [13] D. Rueckert, G. I. Sanchez-Ortiz, and P. Burger. Motion and Deformation Analysis of the Myocardium Using Density and Velocity Encoded MR Images. In *10th International Symposium on Computer Assisted Radiology, CAR'96*, pages 125–130, Paris, June 26-29 1996.
- [14] W.J. Niessen, B.M. ter Haar Romeny, L.M.J. Florack, and M.A. Viergever. A general framework for geometry-driven diffusion equations. *Int. J. of Computer Vision*, pages 1–21, 1995.